Probing double Rydberg wave packets in a helium atom with fast single-cycle pulses

Xiao Wang and F. Robicheaux

Phys. Rev. A **96**, 043409 — Published 11 October 2017

DOI: 10.1103/PhysRevA.96.043409

Probing double Rydberg wave packets in a helium atom with fast single-cycle pulses

Xiao Wang[1] and F. Robicheaux[1,2,*]

[1] *Department of Physics and Astronomy, Purdue University, West Lafayette, Indiana 47907*
[2] *Purdue Quantum Center, Purdue University, West Lafayette, Indiana 47907*

(Dated: September 29, 2017)

Fully quantum and classical calculations on a helium atom with two excited, radially localized Rydberg wave packets are performed. The differences between classical and quantum methods are compared for a wide range of principal quantum numbers to study the validity of the classical method for low-lying states. The effects of fast terahertz single-cycle pulses on an atomic system with one or two Rydberg wave packets are also studied using classical equations of motion. These results suggest that single-cycle pulses can be used as time-resolved probes to detect motion of the wave packets and to investigate autoionization properties.

PACS numbers: 32.80.Ee, 32.80.Qk, 32.80.Zb

I. INTRODUCTION

The study of correlations between two bound electrons has remained an interesting topic since the development of quantum mechanics in the early 20th century. The basic Coulomb form of the interaction is a prototype of coupled degrees of freedom in atomic physics. Thus, understanding the correlations between two electrons can help us understand more complicated atoms and molecules. In recent years, numerous experiments have been done using ultrafast laser pulses to observe, create, and control different two-electron processes [1–5]. Most of them have been focused on resonant transitions in low-lying states.

In contrast to low-lying states, highly excited Rydberg states have many novel properties. The tiny energy spacing between adjacent Rydberg states makes it easier to generate spatially localized Rydberg wave packets [6, 7]. Many experimental and theoretical studies on atoms with a single Rydberg wave packet have been conducted in the past few decades [8–17]. However, there are only a few experimental studies of the dynamics of double Rydberg wave packets [18–22]. Recently, experiments done by Zhang *et al* in Ref. [21] studied the time evolution of two highly excited Rydberg wave packets. Their experimental and numerical results were in good agreement and showed that substantial energy and angular momentum exchanges between the two electrons can happen in just a few Rydberg periods. This motivates us to study the time-dependent dynamics of double Rydberg wave packets, which has not been systematically studied before. A numerical method using basis expansion techniques was introduced in Ref. [23]. Another method [24] based on the time-dependent close coupling method [25] will be used in this report to study the dynamics of double Rydberg wave packets.

Most quantum mechanical methods face computational power issues when dealing with highly excited Rydberg electrons, due to the wide spatial range, long time scale of substantial interactions, and strong mixing among enormous numbers of basis functions. Early research showed that Rydberg electrons behave more classically than electrons in low-lying states [26, 27]. This suggests the use of well-studied classical mechanics to investigate those two-electron atoms. Classical calculations with a wide range of principal quantum numbers are performed in this paper, and the results are compared with quantum calculations to study the validity of the classical method.

Experimentalists have been using well-controlled fast THz pulses as a time-resolved probe to study the Rydberg electronic wave function structures at different times as the system evolves [21, 28, 29]. Durations of fast THz pulses can be modified to be shorter than, equal to, or longer than the period of Rydberg electrons, which can yield totally different field-ionization results. Subpicosecond half-cycle pulses (HCP) have been widely used to probe wave function structures of a single Rydberg wave packet since the 1990s [15, 30, 31], but only a few experiments have been done using HCP to study double Rydberg wave packets [21]. The effects of fast THz single-cycle pulses (SCP) on atoms with one valence electron at different bound states have been studied in both theoretical [32–34] and experimental [28] ways. However, there has been no study on the effect of a SCP on an atom with doubly excited Rydberg wave packets. In this paper, we focus on the use of SCP to obtain wave function structures from double Rydberg wave packets. We can also predict motions of the double Rydberg wave packets from the time-resolved ionization results with SCP.

This paper is organized as follows. In Sec. II, we introduce the two-step launch model for generating double Rydberg wave packets based on experiments in Ref. [21]. Both fully quantum and classical calculations are performed in order to explore the differences between them and the validity of classical methods in low-lying states. In Sec. III, we focus on the effect of a fast SCP on an atomic system. The evolution and autoionization of the double Rydberg wave packets are then studied using a SCP. All physical variables and formulas presented in

* robichf@purdue.edu

this paper are in atomic units unless specified otherwise.

II. COMPARISON BETWEEN FULLY QUANTUM AND CLASSICAL METHODS

A. The two-step launch model

Our theoretical model is motivated by an experiment in Ref. [21], where both valence electrons in Ba are individually excited to Rydberg wave packet type states. The experiment starts with Ba atoms in the ground state, $6s^2$. The atom is excited to a coherent superposition of $5d_{5/2}n_1d$ Rydberg states using two consecutive laser pulses. The first radially localized wave packet is generated as a superposition of n_1 states. Its Rydberg period is about $T_{\rm Ryd1} = 2\pi\nu_1^3$, where $\nu_1 = n_1 - \mu_1$ is the effective principal quantum number. The ν_1 corresponds to the central binding energy $E_1 = -1^2/2\nu_1^2$, and the μ_1 is the quantum defect. When the first wave packet reaches its outer turning point, the other electron is then excited to a Rydberg wave packet giving n_2gn_1d states. The $\nu_2 = n_2 - \mu_2$ is the effective principal quantum number that corresponds to the central binding energy $E_2 = -2^2/2\nu_2^2$. Central energies and energy widths of the two Rydberg wave packets are controlled by properties of laser pulses used to excite the atom. Dynamics of the double Rydberg wave packets can then be studied.

This experiment can be converted into a theoretical two-step launch model in a helium atom. We focus on an easier case where the angular momenta l_j of both electron at launch are zero. Usually, when the total angular momentum L is on the order of 1 and is much smaller than both principal quantum numbers, the dynamics are insensitive to the total angular momentum L. Calculations with different small L are described in Sec. II D. Therefore, the first electron is launched as a spherically symmetric s-wave centered at a negative total energy $E_1 = -1^2/2\nu_1^2$ and a launch time width δt_1. The δt_1 is a time width parameter that describes a Gaussian shaped electric field amplitude, which is $F_1(t) \propto \exp(-2\ln 2\, t^2/\delta t_1^2)$. At $t = 0.5\ T_{\rm Ryd1}$, the second electron is also launched as a spherically symmetric s-wave centered at a negative total energy $E_2 = -2^2/2\nu_2^2$ and a launch time width δt_2. The δt_2 has a similar definition as of δt_1. In the quantum calculations, the energy width is an automatic result of the duration of the laser pulse that excites each wave packet. In the classical calculations, the energy width is selected to be the same as that in the quantum calculations. To satisfy the uncertainty principle, the FWHM of a Gaussian shaped energy distribution of the Rydberg wave packet satisfies $\delta E_j = 4\ln 2/\delta t_j$, where $j = 1, 2$ represent the first and second electron, respectively. We then study the autoionization process of the atom, and angular momenta distributions of the electrons after the second electron's launch.

B. Quantum approach

For a neutral helium atom with two electrons, the Hamiltonian of this system can be written as

$$H = \frac{\mathbf{p_1}^2}{2} + \frac{\mathbf{p_2}^2}{2} - \frac{2}{r_1} - \frac{2}{r_2} + \frac{1}{|\mathbf{r_1} - \mathbf{r_2}|}, \qquad (1)$$

where $\mathbf{p}_j$ and $\mathbf{r}_j$ are the momentum and spatial coordinate of the j-th electron, respectively. The main difference of a helium atom's Hamiltonian compared to a hydrogen atom's is the Coulomb interaction term $1/|\mathbf{r_1}-\mathbf{r_2}|$, which couples the two electrons. In this paper, a method based on the time-dependent close coupling (TDCC) method is used to propagate the wave function of a helium atom [24, 25].

Expanding the two-electron wave function in a coupled spherical harmonic basis, the wave function can be written as

$$\Psi^{LS}(\mathbf{r_1},\mathbf{r_2},t) = \sum_{l_1,l_2} \frac{R^{LS}_{l_1,l_2}(r_1,r_2,t)}{r_1 r_2} \times \sum_{m_1,m_2} C^{l_1,l_2,L}_{m_1,m_2,0} Y_{l_1,m_1}(\hat{r_1}) Y_{l_2,m_2}(\hat{r_2}), \qquad (2)$$

where $R^{LS}_{l_1,l_2}$ is the radial wave function, $C^{l_1,l_2,L}_{m_1,m_2,0}$ is the Clebsch-Gordan coefficient, Y_{lm} are spherical harmonics, r_1, r_2 represent the spatial coordinates of the two electrons [25]. To reduce the computational requirements, the calculation can be performed with total angular momentum $L = 0$ instead of small non-zero total angular momentum. Additionally, since both Rydberg wave packets are highly localized in phase space and far away from the nucleus, the overlap integral and exchange effect are expected to be small. Singlet and triplet symmetrized calculations will give nearly the same result. With total angular momentum $L = 0$, the wave function only depends on r_1, r_2, and the relative angle θ_{12} between $\mathbf{r_1}$ and $\mathbf{r_2}$, [35]. The wave function in Eq. (2) with $L = 0$ can be simplified to

$$\Psi(\mathbf{r_1},\mathbf{r_2},t) = \sum_{l=0}^{L_{\rm max}} (-1)^l R_l(r_1,r_2,t) Y_{l0}(\cos\theta_{12}), \qquad (3)$$

where the $(-1)^l$ term is following the conventions of Refs. [36, 37]. The $L_{\rm max}$ is the number of angular channels used in the calculation, and it's slightly larger than the maximum allowed angular momentum restricted by the total energy. The goal is to evolve the R_l for all coupled channels with different angular momentum l of one electron.

For the time propagation of the wave function, the split-operator technique is used. The Hamiltonian in Eq. (1) can be split into 3 parts, $H_j = p_j^2/2 - 2/r_j$ with $j = 1, 2$ for each electron, and $H_3 = 1/r_{12}$ for the interaction between the two electrons. The unitary propagators of U_1, U_2, and U_3 can be taken in various forms at each time step, e.g. Crank-Nicolson, Chebyshev, or leapfrog,

etc. The propagators U_1 and U_2 don't couple amplitudes R_l with different angular momentum, and are tridiagonal in r_1 and r_2, respectively. For the propagator U_3, the idea from discrete variable representation is used in the calculation [38]. The method is described in Ref. [24] in detail, and we give a brief description here. First, the matrix elements of $\cos\theta_{12}$ in the coupled angular momentum basis $|j\rangle = |(l_j, l_j)L = 0\rangle$ are calculated [36]. Then, the matrix of $\cos\theta_{12}$ is diagonalized, and we can use its eigenstates, eigenvalues and the geometric relation $r_{12} = (r_1^2 + r_2^2 - 2r_1 r_2 \cos\theta_{12})^{1/2}$ to calculate the matrix element of U_3 in the coupled angular basis $|j\rangle$. Finally, the U_3 propagator couples all the angular states $|j\rangle$, and the radial amplitudes R_j are propagated to the next time step.

At the final time of the calculation, we can project the calculated wave function onto energy eigenstates of a helium atom to get the energy distribution. Since the total angular momentum of the system is zero, angular momenta of the two electrons have the same magnitude but in the opposite directions. The angular momentum distribution of one electron is calculated using [37]

$$p_{\rm qm}(l) = \iint {\rm d}r_1 {\rm d}r_2 \Big| R_l(r_1, r_2, t) \Big|^2 . \qquad (4)$$

C. Classical approach

The three-dimensional classical trajectory Monte Carlo (CTMC) method [15, 24, 39, 40] is used in the calculations as a comparison with the quantum calculation, as a way of interpreting the results, and as a way to obtain results difficult or impossible to converge using quantum calculations. Initial conditions of the electrons are set to obey the quantum uncertainty principle with random Gaussian distributed energies and launch times. Since both electrons are launched as spherically symmetric s-waves, their launch directions are uniformly distributed in all 4π solid angle.

After the initial launches, the system is propagated under Hamilton's equations using a fourth order Runge-Kutta method with adaptive step size [41]. To avoid divergence near the nucleus, a soft core potential $V(r) = -Z/\sqrt{r^2 + a^2}$ is used instead of $V(r) = -Z/r$ for the Coulomb interactions, where a is a soft core parameter. Calculations performed with a ranged from 1.0×10^{-3} to 1.0×10^{-5} give converged results.

At the final time of the calculations, the statistics of energies, angular momenta, and other physical quantities of each electron from all Monte Carlo (MC) runs with different initial conditions give continuous distribution functions. The continuous distribution functions can be discretized and compared to the quantum calculations. For example, the classical analogy of the probability of the angular momentum at l_c can be calculated as follows

$$p_{\rm cl}(l_c) = \frac{\text{Number of MC runs with } l_c \leqslant l < l_c + 1}{\text{Total number of MC runs}}, \qquad (5)$$

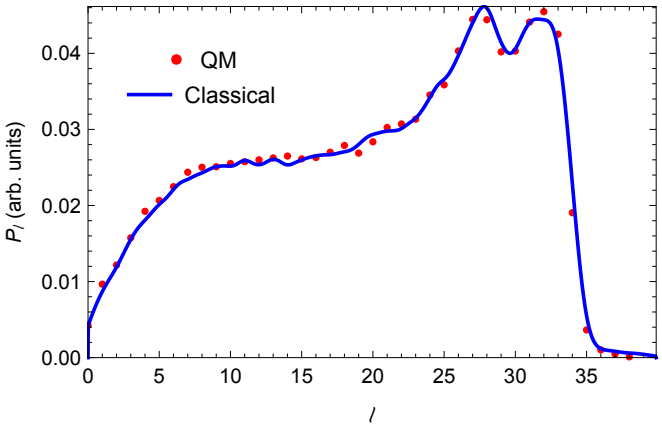

FIG. 1. Comparison between the quantum and classical methods for the angular momentum distribution. The effective principal quantum numbers are $\nu_1 = 23$, $\nu_2 = 38$, which correspond to central energies $E_1 = -1^2/2\nu_1^2 = -9.45 \times 10^{-4}$, $E_2 = -2^2/2\nu_2^2 = -1.39 \times 10^{-3}$ at launch. Rydberg period of the first electron is $T_{\rm Ryd1} = 2\pi\nu_1^3 = 7.64 \times 10^4$. The 2nd electron is launched at half of the Rydberg period of the 1st electron after the 1st electron's launch. Launch time widths for the two electrons are $\delta t_1 = 2.17 \times 10^4 = 0.28\, T_{\rm Ryd1}$, $\delta t_2 = 4.28 \times 10^3 = 0.056\, T_{\rm Ryd1}$, which are shorter than a full Rydberg period. The results in the figure are at $t = 8.27 \times 10^4$ a.u. after the 2nd launch, which is about 2 picosecond.

where l is the angular momentum from the classical calculations. The l_c is a non-negative integer, which corresponds to the azimuthal quantum number in the quantum calculations. The $p_{\rm cl}(l_c)$ is compared to the quantum angular momentum distributions $p_{\rm qm}(l_c)$, to study the differences between the classical and quantum methods.

D. Comparisons between quantum and classical methods

To study the validity of the classical methods, we start this subsection with a calculation for $\nu_1 = 23$, $\nu_2 = 38$. The principal quantum numbers are chosen to be neither too large, where the quantum calculations would be hard to converge, nor too small, where the quantum effects can cause huge differences between the quantum and classical calculations. Comparison of angular momentum distributions between quantum and classical methods can be found in Fig. 1, with all the corresponding parameters given in the caption. In this calculation, the total angular momentum is set to zero. The results presented here are for the non-ionized part of the wave function, which is only about 30% at the final time of 2 ps. The numerical difference for ionization probabilities between the classical and quantum methods is about 1% at the final time. The final time of this calculation is about one Rydberg period of the first electron. In this time scale, significant interactions between the two electrons

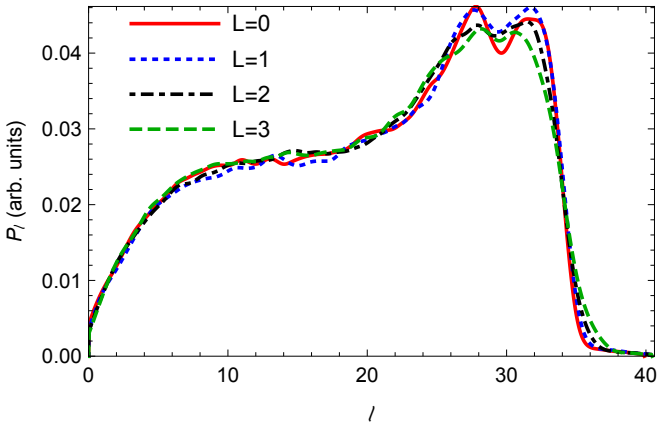

FIG. 2. Comparison of the angular momentum distributions between classical calculations with total angular momentum $L = 0, 1, 2, 3$. All the parameters are the same as those given in the caption of Fig. 1 except for the total angular momentum. Since the total angular momentum is non-zero, the angular momenta of the two electrons have a small difference. The separate angular momentum distributions of the two electrons have no visible differences, thus their distributions are plotted on a single curve as shown in the figure.

can happen. This leads to a large probability of autoionization, and can excite most of the two-electron wave function to high angular momentum states. In the figure, a sharp decrease in angular momentum distribution can be found near $l = 36$, which is the maximum classically allowed angular momentum when both electrons are bound [42].

Additionally, classical calculations that the second electron starts at a non-zero angular momentum are performed. The results also match well with the $L = 0$ results, and can be found in Fig. 2. The calculations with non-zero total angular momentum strengthen our assumption that the dynamics of Rydberg electrons is insensitive to small non-zero angular momentum.

With the comparison between quantum and classical calculations for highly excited states, the principal quantum number is then lowered, to study the validity of the classical methods at low-lying states. We define a *difference function* to quantitatively study the differences between the two methods for different principal quantum numbers. The difference function f_d is defined as

$$f_d = \sum_{l=0}^{L_{\max}} \Big| p_{\rm cl}(l) - p_{\rm qm}(l) \Big|, \qquad (6)$$

where $L_{\max}$ is the number of coupled angular channels used in the quantum calculations. The $p_{\rm qm}(l)$ is the probability that the electron has an angular momentum l as defined in Eq. (4) in quantum calculations. The $p_{\rm cl}(l)$ is an analogous probability that the electron has an integer angular momentum l in classical calculations, which is defined in Eq. (5). The difference function gives an estimation on the relative error between the two methods at different l. The higher f_d is, the larger differences between the quantum and classical methods are.

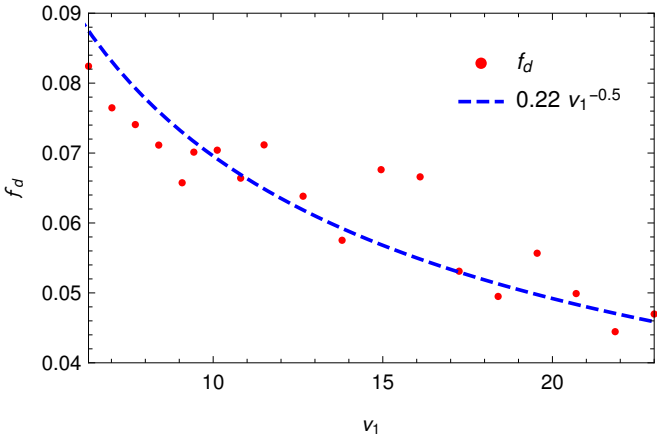

FIG. 3. The difference function f_d as defined in Eq. (6) versus the first electron's principal quantum number ν_1. In these calculations, the principal quantum numbers of the two electrons satisfy $\nu_1/\nu_2 = 23/38$. The red dots are the numerical results for the f_d, while the blue line is a fit for the numerical results versus ν_1.

Fully scaled calculations with $\nu_1 = 23\zeta$, $\nu_2 = 38\zeta$ have been performed, where $0 < \zeta \leqslant 1$ is a dimensionless number. The laser time widths are scaled as ζ^3, since the Rydberg period of an electron and the interval between the two electrons' launches are proportional to cube of their principal quantum numbers. To satisfy the quantum uncertainty principle, the energy widths are scaled as ζ^{-3} in both classical and quantum calculations. Final time of the calculations are also scaled as ζ^3. Similar to the calculation for ν_1, $\nu_2 = 23$, 38, the angular momentum distributions used in Eq. (6) are only from the non-ionized part of the wave function.

The results of the difference function versus the first electron's principal quantum number ν_1 can be found in Fig. 3. In the figure, as the principal quantum number decreases, the difference between the two methods increases. Due to the interference and tunneling effects that only exist in quantum mechanics, the difference between the two methods fluctuates as the energy of the system changes. Also, finite energy spacings in the quantum calculations and finite final time of the calculations may cause additional disagreements between the quantum and classical methods [43, 44]. We use n to denote the principal quantum number of the atomic system. Since the energy spacings between adjacent Rydberg states are also scaled as n^{-3} as energy uncertainties, approximately same number of quantum states are included in a Rydberg wave packet regardless of n. However, as n gets smaller, the discretized energy levels in quantum mechanics may cause totally different behaviors from continuous energies in classical mechanics, which could result in a difference function that scales as power of n. A rough fit of the f_d is also given in the figure, and that indicates the differences between classical and

quantum calculations scale as $n^{-1/2}$. There are not many studies on the differences between classical and quantum calculations for different principal quantum numbers in an atomic system. Related studies on the differences in other systems can be found in Refs. [44–46].

III. PROBING DOUBLE RYDBERG WAVE PACKETS

Properties of double Rydberg wave packets in an atomic system are well described by classical calculations. To avoid the huge computational effort on mixing of large number of angular momentum states in quantum calculations, all of the following calculations related to single-cycle pulses (SCP) are classical calculations.

A. The effect of SCP on a one electron atom

We start this subsection with a study of the effect of short SCP on an atomic system with one Rydberg electron. A Rydberg electron is prepared in a classical, elliptical Rydberg orbit with a small angular momentum. The electron has a significant time to be far away from the nucleus, and a relatively short time to be close to the nucleus in its one Rydberg period. The electric field of a SCP in our calculation has the following form

$$F(t) = C_0 F_m \left(\frac{t}{t_w}\right) \exp\left[-\left(\frac{t}{t_w}\right)^2\right], \qquad (7)$$

where $C_0 = \sqrt{2e} \approx 2.332$ is a constant to make the maximum field strength be F_m, note that e here is the base of natural logarithms. The t_w is a parameter to characterize the duration of the pulse. In our calculations, a SCP starts at $t = -3.5\,t_w$, and ends at $t = +3.5\,t_w$. A SCP has a duration $T_{\rm pulse} = 7.0\,t_w$. Durations of the short pulses in the calculations below are much shorter than or equal to one Rydberg period of the electron. Effects of a SCP in these two scenarios can be totally different. Single-cycle pulses are applied to a one-electron atom at different times, and the energy distributions of the electron after the SCP are observed.

We first describe the effect of a SCP with duration much shorter than one Rydberg period. Within the duration of a short SCP, the nucleus-electron interaction can be neglected if the electron is far away from the nucleus. Since the integral of the electric field over time is zero, a short SCP only shifts the position of the electron, and has almost no effect on its kinetic energy. The estimated energy change of the electron originates from the Coulomb potential energy change. If the electron was close to the nucleus before the SCP, the potential energy change is much higher than that for an electron which was far away from the nucleus. This is equivalent to saying that a short SCP transfers more energy to an atom when an electron is closer to the nucleus at the time of the SCP.

We also study the effect of a SCP with duration equal to one Rydberg period. The electric field of a SCP has maximum amplitude at $t = \pm\, t_w/\sqrt{2} \approx \pm\, 0.707\, t_w$, which is about half of its duration. If a SCP starts at the time that the electron is close to the nucleus, the electron feels maximum accelerations when it moves to the Rydberg outer turning point. Acceleration from the SCP quickly flips the sign at almost the same time that the electron passes the outer turning point, and reverses its moving direction. This means the SCP can perfectly accelerate the electron during the whole pulse. This is also true if a SCP starts at the time that the electron is close to the outer turning point. However, there is a main difference between these two scenarios. The work done to the electron is the integral of force times displacements. The electron moves much faster when it is close to the nucleus than far away from the nucleus. Using pulses with same strengths, the absolute value of the work done by a SCP is much larger when it starts at the time that the electron is at its outer turning point.

To summarize, a short SCP transfers more energy when the electron is close to the nucleus, while a medium duration SCP transfers more energy when it starts at the time that the electron is far away from the nucleus. An atom can be ionized if the final energy after a SCP is above the ionization threshold. In experiments, a SCP can be used to probe the periodic motion of the Rydberg wave packet in a one electron atom.

B. Probing double Rydberg wave packets

Within our two-step launch model described in Sec. II A, dynamics of the double Rydberg wave packets can be divided into two regions based on their initial energies. (i) One wave packet has a much larger Rydberg orbit than the other. This means the two wave packets are usually spatially distinguishable, with an inner wave packet and an outer wave packet. (ii) Two wave packets have similar sized Rydberg orbits. We apply a fast SCP at different times after the electron launches. The SCP can transfer energy to the atomic system. At a long final time, the atom will be singly or doubly ionized. In our following calculations, the double ionization probabilities are very small and can be neglected. We can measure the energy distributions of those singly ionized atoms to study the electronic wave function structures at the start time of the SCP.

A classical calculation with $\nu_1 = 45$, $\nu_2 = 38$ has been performed. This leads to the initial energies $E_{1i} = -2.47 \times 10^{-4}$, $E_{2i} = -1.39 \times 10^{-3}$, and Rydberg periods $T_{\rm Ryd1} = 13.8$ ps, $T_{\rm Ryd2} = 2.08$ ps. Before the first wave packet returns to the nucleus ($0.5\,T_{\rm Ryd1} = 6.9$ ps), the second electron is expected to be in its own periodic motion around the nucleus. In this calculation, the first electron is considered as the outer wave packet, while

the second electron is the inner wave packet. A short SCP with duration $T_{\rm pulse} = 0.208$ ps $\approx 0.1\ T_{\rm Ryd2}$, and maximum strength $F_m = 100$ kV/cm is applied at different times ($t_{\rm start}$) after the second launch. Distributions of the positive ion's final energy, E_+, can be found in Fig. 4. In the figure, most of the energy distributions are lower than E_c, center of the initial total energy shifted by energy widths, which is indicated as the vertical dashed line. For these electrons with $E_+ > E_c$, the atom must have gained energy from the SCP. As our analyses in Sec. III A, a short SCP transfers more energy to an atom through the inner electron when the electron is close to the nucleus. If the energy transferred to the inner electron is large enough, the inner electron can be directly ripped off from the atom. In this scenario, there will be no further chaotic three-body interactions after the outer electron returns. The energy of the outer electron after the inner electron being ionized should be approximately $2E_{1i}$, which originates from the changing of ionic core charge from 1 to 2. In Fig. 4, when $E_+ > E_c$, the peak of the positive ion's energy is located at $2E_{1i}$.

To further study our claim that a short SCP transfers energy to an atom when the electron is close to the nucleus, we plot the probability of $E_+ > E_c$ versus $t_{\rm start}$ in Fig. 5. The probability indicates direct ionization of the inner electron due to the short SCP. Additionally, we calculate the probability that at least one electron is within a sphere of $R_c = 260$ au centered at the nucleus, when neither electron is autoionized before the pulse. The latter probability, P_c, versus $t_{\rm start}$ is plotted in Fig. 5. The R_c is calculated to satisfy

$$\frac{-2}{R_c + \Delta r} - \frac{-2}{R_c} + E_c \geqslant 0, \tag{8}$$

where Δr is the displacement of a free electron due to a SCP. The probabilities of $E_+ > E_c$ and P_c have similar trends and magnitudes on the locations of peaks and troughs. To study the origin of P_c, we calculated the probabilities that each electron is within R_c, indicated with P_{c1} and P_{c2} for the first and second electron, respectively. The plots can be found in Fig. 5. Note that, the probability that both electrons are within R_c is less than 0.1% and can be neglected here, which means $P_c \approx P_{c1} + P_{c2}$. The peaks of P_{c2} are located at $t_{\rm start} \approx 2.0, 4.0, 6.0$ ps, which are multiples of $T_{\rm Ryd2}$ and indicate the inner electron's return to the nucleus. Similarly, the outer electron returns to the nucleus at $t_{\rm start} \approx 6.9$ ps. Instead of a peak in P_{c1} at 6.9 ps, we can find a small dip on it. This is because at $t_{\rm start} \approx 7.0$ ps, the inner electron is at its outer turning point. Thus, the repulsion between the inner electron and the returning outer electron shifts the radial positions of the two electrons. Therefore, P_{c1} is slightly lower and P_{c2} is slightly higher at $t_{\rm start} \approx 7.0$ ps. On the P_{c2} curve at 7.0 ps, the depth of the dip is not as large as that at 5.0 and 8.0 ps. As a result, we have flatter distributions near 7.0 ps on both P_c and $E_+ > E_c$ curves. After 8.0 ps, both curves are mostly flat, indicating a SCP applied after the collisions between the two electrons. The probability to find electrons in a small radial range barely changes after collision.

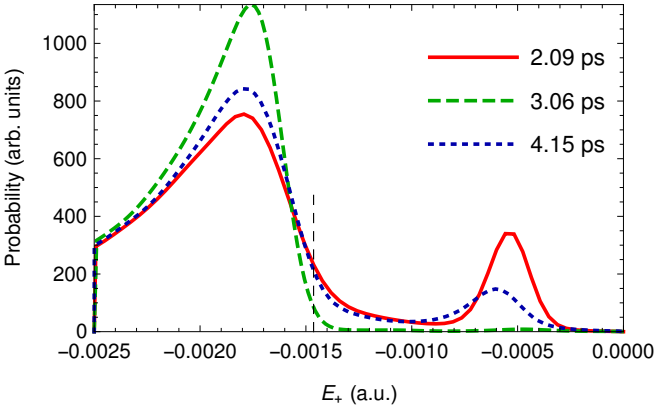

FIG. 4. Energy distributions of the electron in a singly ionized ion at a long final time, after the effect of a short SCP applied at different time. The principal quantum numbers for the two electrons are $\nu_1 = 45$, $\nu_2 = 38$. The SCP has a maximum strength $F_m = 100$ kV/cm, and a duration $T_{\rm pulse} = 0.208$ ps. Numbers in the legends indicate the start time of SCP ($t_{\rm start}$) after the launch of the second electron. The vertical dashed line is plotted at $E_c = -1.46 \times 10^{-3}$. The figure has a cutoff at -0.0025 on the left, but the full energy distributions have long tails to larger binding energies.

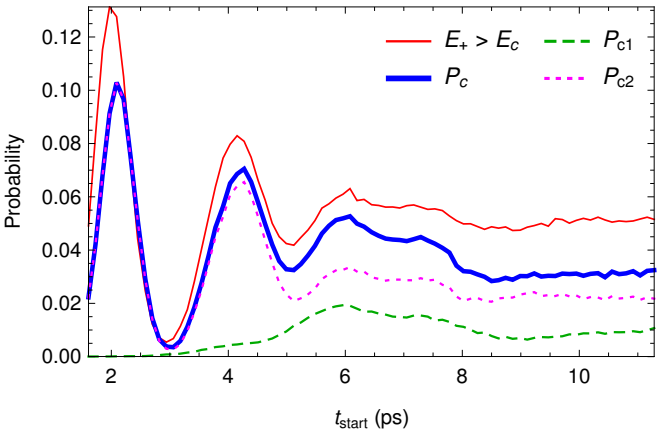

FIG. 5. Probability results for calculations with $\nu_1 = 45$, $\nu_2 = 38$, $F_m = 100$ kV/cm, $T_{\rm pulse} = 0.208$ ps. The red thin solid line describes the probability of $E_+ > E_c$, which is the positive ion's final energy higher than -1.46×10^{-3}, with a short SCP applied at different time $t_{\rm start}$. The blue thick solid line describes the probability that at least one electron is within $R_c = 260$, at different time $t_{\rm start}$ after the second electron's launch, just before the application of a SCP. The green dashed line describes the probability that the first electron is within R_c at different time, while the magenta dotted line describes the probability for the second electron.

To study the effect of a medium duration SCP, calculations with $\nu_1 = 45$, $\nu_2 = 40$, $T_{\rm pulse} = 2.43$ ps $\approx 1.0\ T_{\rm Ryd2}$ and $F_m = 5$ kV/cm, have been performed. For this case, the $T_{\rm pulse}$ is smaller than the outer electron's Rydberg

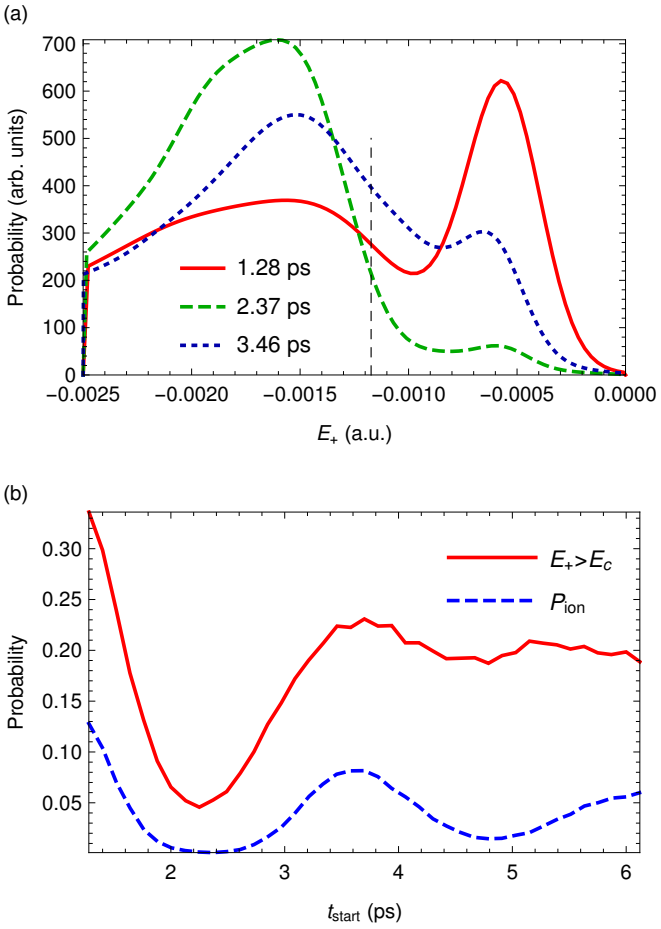

FIG. 6. Study of the effect of a medium duration SCP with $\nu_1 = 45$, $\nu_2 = 40$, $F_m = 5$ kV/cm, and $T_{\rm pulse} = 2.43$ ps. Figure (a) describes the same physical quantities as given in the caption of Fig. 4. Figure (b) describes the probability of positive ion's energy higher than $E_c = -1.17 \times 10^{-3}$, and the direct ionization probability of a He^+ ion due to a medium duration SCP with same properties. The $t_{\rm start}$ is the start time of a medium duration SCP (see Eq. (7) for definition of the start time).

period $T_{\rm Ryd1}$. When the outer electron is far away from the nucleus, the SCP only slightly shifts its position, and has negligible effect on it. We may only consider the effect of the SCP on the inner electron, before the outer electron returns. Energy distributions of the positive ion at a long final time can be found in Fig. 6(a), which has the same meaning as described in Fig. 4. The probability of $E_+ > E_c$ can be found in Fig. 6(b). To have a detailed understanding of the effect of a medium duration SCP, we have performed calculations of a He^+ ion with only one Rydberg wave packet at $\nu_2 = 40$ under the effect of a same medium duration SCP, with $T_{\rm pulse} = 2.43$ ps and $F_m = 5$ kV/cm, applied at different times. The field induced ionization probability ($P_{\rm ion}$) of the He^+ is also plotted in Fig. 6. At $t_{\rm start} = 2.4$ ps $\approx 1.0\ T_{\rm Ryd2}$, the electron in He^+ model and the inner electron in the two-electron atom return to the nucleus, and gain the lowest energy transferred from a short SCP. Thus the probabilities of $E_+ > E_c$ and $P_{\rm ion}$ reach their minimum. Similarly, at $t_{\rm start} = 1.3$ ps $\approx 0.5\ T_{\rm Ryd2}$ and $t_{\rm start} = 3.5$ ps $\approx 1.5\ T_{\rm Ryd2}$, the electron in He^+ model and the inner electron in the two-electron atom are at their outer turning points, and $E_+ > E_c$, $P_{\rm ion}$ reach their maximum. These two lines have very similar trends, which strengthens our assumption that a medium duration SCP transfers more energy to an atom when it starts at the time that the electron is far away from the nucleus.

These calculations show that single-cycle pulses with a short duration and a medium duration behave oppositely on the energy transfer to a Rydberg electron. Experimentally, a SCP can be used to probe the wave function structures of the inner wave packet, by transferring energy to the atom through the inner electron while the inner electron is located at different positions.

C. Atoms with similar sized double Rydberg wave packets

In the previous subsection, we studied the effect of a SCP on a two-electron atom with the size of one Rydberg wave packet much larger than the other's. Here we focus on those scenarios that the two Rydberg wave packets have similar sizes. A classical calculation with $\nu_1 = 34$, $\nu_2 = 40$ has been performed. The single-cycle pulses have durations $T_{\rm pulse} = 0.1\ T_{\rm Ryd2} = 0.243$ ps, and maximum strengths $F_m = 100$ kV/cm. The $E_c = -1.42 \times 10^{-3}$ is center of the initial total energy shifted by energy widths. The probability of $E_+ > E_c$, versus different start time of the SCP is plotted in Fig. 7. The probabilities to find electrons within $R_c = 300$ au, P_c, P_{c1}, P_{c2}, as introduced in the previous subsection can also be found in Fig. 7. In the figure, similar trends between $E_+ > E_c$ and P_c can be found, which is because a short SCP transfers more energy to an electron when it's close to the nucleus. The peak of P_{c1} is located at $t_{R1} = 2.4$ ps, which indicates the first electron's return to the nucleus. Similarly, the second electron returns to the nucleus at $t_{R2} = 3.4$ ps. These return times are neither a full nor a half Rydberg period related to their initial energies. Due to the correlations between the two electrons, their energies, angular momenta, and Rydberg periods are changed.

After the two electrons return to the nucleus, respectively, they will be in Rydberg orbits with new periods. The new periods are approximately $2\,t_{R1}$ and t_{R2} for the two electrons, which can be deduced from the peaks and troughs on the P_{c1} and P_{c2} curves in Fig. 7. The first electron arrives at its new outer turning point at about $2\,t_{R1} = 4.8$ ps, while the second electron arrives at its new outer turning point at about $1.5\,t_{R2} = 5.1$ ps. As can be seen in Fig. 7, at $t_{\rm start} \approx 4.8$ ps, the probabilities to find either electron inside R_c are at minimum. The energy transferred from a short SCP and the probability of $E_+ > E_c$ are also at local minimum.

Experimentally, a short SCP can be used to probe an

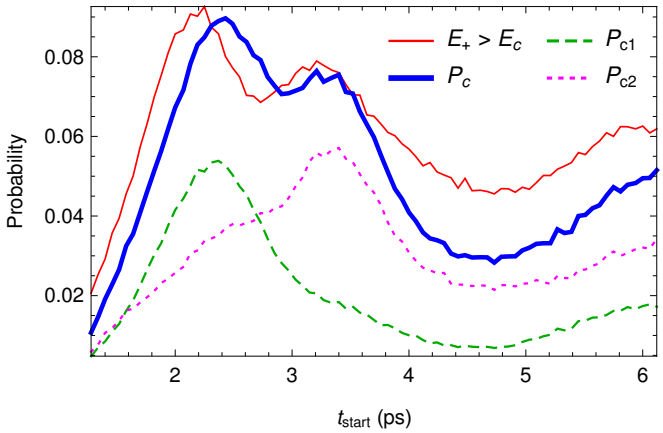

FIG. 7. The curves have the same meaning as introduced in the caption of Fig. 5. Parameters used in the plot are $\nu_1 = 34$, $\nu_2 = 40$, $F_m = 100$ kV/cm, $T_{\rm pulse} = 0.243$ ps, $E_c = -1.42 \times 10^{-3}$, and $R_c = 300$.

atom with two similar sized Rydberg wave packets. Usually, the first two peaks of the probability of $E_+ > E_c$ indicate the return times of the two electrons. After that, the two electrons will be in new Rydberg periods which are related to their first return times to the nucleus.

IV. CONCLUSIONS

Inspired by a previous experiment in Ref. [21], and various numerical methods for solving two-electron atoms developed in the past few years, we studied dynamics of two Rydberg wave packets in a helium atom. We first briefly introduced the helium model with two-step launches, where the first electron was excited to a radially localized Rydberg wave packet using laser pulses with tunable parameters. When the first electron reached its outer turning point, the other electron was then excited to a Rydberg wave packet using laser pulses with different properties. As studied in Ref. [21], energy and angular momentum exchanges between the two electrons can happen quickly, leading to rapid autoionization.

We then performed both quantum and classical calculations to show the validity of the classical methods when dealing with Rydberg wave packets, comparing to an accurate quantum method. The classical and quantum methods were in good agreement at high principal quantum numbers. The numerical differences between the two methods at lower principal quantum numbers were also quantitatively studied.

Furthermore, we introduced the effects of a fast single-cycle pulse on an atom with one Rydberg electron. Detailed analyses showed that, a short duration single-cycle pulse transfers more energy to an atom when the electron is closer to the nucleus, while a medium duration single-cycle pulse transfers more energy when it starts at the time that the electron is further away from the nucleus. With these results, we studied the effects of a single-cycle pulse on an atom with double Rydberg wave packets. A short single-cycle pulse is applied to an atomic system with distinguishable wave packets at different time, and the energy distribution of the positive ion at a long final time is measured. The probability that significant energy is transferred to the atom has a very similar trend as the probability that at least one electron is located in a small region very close to the nucleus. We also compared the results of a single-cycle pulse acting on an atom with double wave packets of significantly different sizes, and on a positive ion with only the inner wave packet. The results have very similar trends which verify our assumptions that a fast single-cycle pulse only has small affects on the outer electron. Moreover, we studied the case that the two Rydberg wave packets have similar sizes. From the time-dependent probabilities that each electron is close to the nucleus, we found out the return times of the two electrons. Due to the correlations between the two electrons, return times of the two electrons are different from their initial Rydberg periods. The new Rydberg periods after both electrons return to the nucleus are related to their return times. Experimentally, a fast single-cycle pulse can be applied at these times that an electron is close to the nucleus, and a large amount of energy will be transferred to the atom. Further novel autoionization behaviors after the effects of single-cycle pulses remain open questions to be studied in both theoretical and experimental ways.

ACKNOWLEDGMENTS

The authors would like to thank Dr. Baochun Yang for helpful discussions. This material is based upon work supported by the U.S. Department of Energy, Office of Science, Basic Energy Sciences, under Award No. DE-SC0012193. This research was supported in part through computational resources provided by Information Technology at Purdue University, West Lafayette, Indiana.

[1] L. Argenti, R. Pazourek, J. Feist, S. Nagele, M. Liertzer, E. Persson, J. Burgdörfer, and E. Lindroth, Phys. Rev. A **87**, 053405 (2013).
[2] A. Jiménez-Galán, F. Martín, and L. Argenti, Phys. Rev. A **93**, 023429 (2016).
[3] J. Feist, S. Nagele, C. Ticknor, B. I. Schneider, L. A. Collins, and J. Burgdörfer, Phys. Rev. Lett. **107**, 093005 (2011).
[4] A. Jiménez-Galán, L. Argenti, and F. Martín, Phys. Rev. Lett. **113**, 263001 (2014).

[5] L.-Y. Peng, W.-C. Jiang, J.-W. Geng, W.-H. Xiong, and Q. Gong, Physics Reports **575**, 1 (2015).

[6] J. Parker and C. R. Stroud, Physica Scripta **1986**, 70 (1986).

[7] W. A. Henle, H. Ritsch, and P. Zoller, Phys. Rev. A **36**, 683 (1987).

[8] L. D. Noordam, D. I. Duncan, and T. F. Gallagher, Phys. Rev. A **45**, 4734 (1992).

[9] G. Alber, H. Ritsch, and P. Zoller, Phys. Rev. A **34**, 1058 (1986).

[10] W. A. Henle, H. Ritsch, and P. Zoller, Phys. Rev. A **36**, 683 (1987).

[11] A. ten Wolde, L. D. Noordam, A. Lagendijk, and H. B. van Linden van den Heuvell, Phys. Rev. Lett. **61**, 2099 (1988).

[12] J. J. Mestayer, B. Wyker, J. C. Lancaster, F. B. Dunning, C. O. Reinhold, S. Yoshida, and J. Burgdörfer, Phys. Rev. Lett. **100**, 243004 (2008).

[13] M. Campbell, T. Bensky, and R. Jones, Opt. Express **1**, 197 (1997).

[14] J. B. M. Warntjes, F. Robicheaux, J. M. Bakker, and L. D. Noordam, The Journal of Chemical Physics **111**, 2556 (1999).

[15] C. O. Reinhold, J. Burgdörfer, M. T. Frey, and F. B. Dunning, Phys. Rev. A **54**, R33 (1996).

[16] D. G. Arbó, C. O. Reinhold, J. Burgdörfer, A. K. Pattanayak, C. L. Stokely, W. Zhao, J. C. Lancaster, and F. B. Dunning, Phys. Rev. A **67**, 063401 (2003).

[17] R. Jones and L. Noordam, Advances In Atomic, Molecular, and Optical Physics **38**, 1 (1998).

[18] S. N. Pisharody and R. R. Jones, Science **303**, 813 (2004).

[19] S. N. Pisharody and R. R. Jones, Phys. Rev. Lett. **91**, 203002 (2003).

[20] A. L. Landers, F. Robicheaux, T. Jahnke, M. Schöffler, T. Osipov, J. Titze, S. Y. Lee, H. Adaniya, M. Hertlein, P. Ranitovic, I. Bocharova, D. Akoury, A. Bhandary, T. Weber, M. H. Prior, C. L. Cocke, R. Dörner, and A. Belkacem, Phys. Rev. Lett. **102**, 223001 (2009).

[21] X. Zhang, R. R. Jones, and F. Robicheaux, Phys. Rev. Lett. **110**, 023002 (2013).

[22] B. J. Lyons, D. W. Schumacher, D. I. Duncan, R. R. Jones, and T. F. Gallagher, Phys. Rev. A **57**, 3712 (1998).

[23] F. Robicheaux and R. C. Forrey, Journal of Physics B: Atomic, Molecular and Optical Physics **38**, S363 (2005).

[24] F. Robicheaux, Journal of Physics B: Atomic, Molecular and Optical Physics **45**, 135007 (2012).

[25] M. S. Pindzola, F. Robicheaux, S. D. Loch, J. C. Berengut, T. Topcu, J. Colgan, M. Foster, D. C. Griffin, C. P. Ballance, D. R. Schultz, T. Minami, N. R. Badnell, M. C. Witthoeft, D. R. Plante, D. M. Mitnik, J. A. Ludlow, and U. Kleiman, Journal of Physics B: Atomic, Molecular and Optical Physics **40**, R39 (2007).

[26] J. G. Leopold and I. C. Percival, Journal of Physics B: Atomic and Molecular Physics **13**, 1037 (1980).

[27] G. Tanner, K. Richter, and J.-M. Rost, Rev. Mod. Phys. **72**, 497 (2000).

[28] S. Li and R. R. Jones, Phys. Rev. Lett. **112**, 143006 (2014).

[29] T. Zhou, S. Li, and R. R. Jones, Phys. Rev. A **89**, 063413 (2014).

[30] C. Raman, C. W. S. Conover, C. I. Sukenik, and P. H. Bucksbaum, Phys. Rev. Lett. **76**, 2436 (1996).

[31] R. R. Jones, Phys. Rev. Lett. **76**, 3927 (1996).

[32] B. C. Yang and F. Robicheaux, Phys. Rev. A **90**, 063413 (2014).

[33] B. C. Yang and F. Robicheaux, Phys. Rev. A **91**, 043407 (2015).

[34] T. Gallagher, *Rydberg Atoms*, Cambridge Monographs on Atomic, Molecular and Chemical Physics (Cambridge University Press, 2005).

[35] A. Edmonds, *Angular Momentum in Quantum Mechanics*, Investigations in Physics Series (Princeton University Press, 1996).

[36] D. Varshalovich, A. Moskalev, and V. Khersonskii, *Quantum Theory of Angular Momentum* (World Scientific Pub., 1988).

[37] Q. Wang, S. Sheinerman, and F. Robicheaux, Journal of Physics B: Atomic, Molecular and Optical Physics **47**, 215003 (2014).

[38] D. O. Harris, G. G. Engerholm, and W. D. Gwinn, The Journal of Chemical Physics **43**, 1515 (1965).

[39] C. O. Reinhold and J. Burgdorfer, Journal of Physics B: Atomic, Molecular and Optical Physics **26**, 3101 (1993).

[40] R. E. Olson and A. Salop, Phys. Rev. A **16**, 531 (1977).

[41] W. Press, *Numerical Recipes 3rd Edition: The Art of Scientific Computing* (Cambridge University Press, 2007).

[42] The maximum classically allowed angular momentum l when both electrons are bound can be calculated using energy conservation, which is $0.5v_{1r}^2 + 0.5v_{2r}^2 + l^2/2r_1^2 + l^2/2r_2^2 - 2/r_1 - 2/r_2 + 1/r_{12} = E_{\rm tot}$. When the radial velocities $v_{r1} = v_{r2} = 0$, $r_{12} = r_1 + r_2$, and $r_1 = r_2 = -7/(4E_{\rm tot})$, the l reaches its maximum $7/(4\sqrt{-E_{\rm tot}})$.

[43] E. J. Heller, The Journal of Chemical Physics **72**, 1337 (1980).

[44] M. J. Davis and E. J. Heller, The Journal of Chemical Physics **80**, 5036 (1984).

[45] E. Kluk, M. F. Herman, and H. L. Davis, The Journal of Chemical Physics **84**, 326 (1986).

[46] A. GarcaVela, R. B. Gerber, and D. G. Imre, The Journal of Chemical Physics **97**, 7242 (1992).